Microfacet Models for Refraction through Rough Surfaces

Bruce Walter[1][†]   Stephen R. Marschner[1]   Hongsong Li[1,2]   Kenneth E. Torrance[1]

[1] Program of Computer Graphics, Cornell University   [2] Beijing Institute of Technology

Abstract
Microfacet models have proven very successful for modeling light reflection from rough surfaces. In this paper we review microfacet theory and demonstrate how it can be extended to simulate transmission through rough surfaces such as etched glass. We compare the resulting transmission model to measured data from several real surfaces and discuss appropriate choices for the microfacet distribution and shadowing-masking functions. Since rendering transmission through media requires tracking light that crosses at least two interfaces, good importance sampling is a practical necessity. Therefore, we also describe efficient schemes for sampling the microfacet models and the corresponding probability density functions.

Categories and Subject Descriptors (according to ACM CCS): I.3.7 [Three-Dimensional Graphics and Realism]:
Keywords: Refraction, Microfacet BTDF, Cook-Torrance Model, Global Illumination, Monte Carlo Sampling

1. Introduction

Transmission into or through refractive media is an important component in the appearance of many materials, including both largely transparent media, such as glass or water, and translucent media, such as skin or marble. When the boundary of a medium is smooth, then transmission is easily modeled using Snell's law of refraction. However, when the boundary is rough, there is a lack of physically based and verified models for use in computer graphics.

In this paper we first review microfacet theory and show how, using a generalization of the half vector, it can be used to model both reflection and refraction at rough boundaries between media. This provides a complete analytic BSDF model that can be used to simulate rough transmissive materials such as the etched glass globe shown in Figure 1. One of our goals is to serve as a complete, self-contained reference for implementors, so we provide all the necessary equations and discuss practical issues such as choices of distributions, shadowing-masking, and importance sampling. Since transmitted light must cross at least two interfaces, good importance sampling is crucial for efficient rendering.

We also validate the microfacet model by comparing it to measured transmission data from four real surfaces. Rough transmission shows several interesting behaviors (e.g., see Figure 2) such as the strong shift in the peak away from the smooth refraction direction towards grazing angles (similar

to off-specular peaks in rough reflection), and the microfacet models are able to successfully predict such effects. We also introduce a new microfacet distribution, which we call GGX, that provides a closer match for some of our surfaces than the standard Beckmann distribution function.

Next we will discuss related work, and then review gen-

Figure 1: *Glass sphere with etched map of the world, simulated using our microfacet refraction model (Beckmann distribution with roughness modulated by a texture map).*

[†] email: {bjw,srm}@graphics.cornell.edu,{hl86,ket1}@cornell.edu

Measured transmission for $\theta_i = 0, 30, 60, 80°$
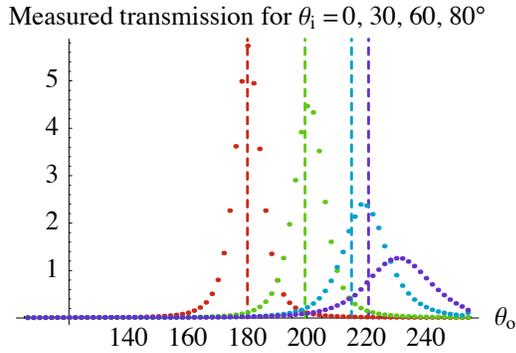
Figure 2: *Measured transmission ($f_t(\mathbf{i}, \mathbf{o}, \mathbf{n})|\mathbf{o} \cdot \mathbf{n}|$) for a rough surface (ground glass) at 0, 30, 60, and 80 degrees incidence angle. Dashed lines are the refracted directions predicted by Snell's law for a smooth surface. Note that the transmitted lobe grows broader as the incidence angle increases and is shifted significantly towards grazing compared to refraction through a smooth surface.*

$\mathbf{i}$	Direction from which light is incident
$\mathbf{o}$	Direction in which light is scattered
$\mathbf{n}$	Macrosurface normal
$\mathbf{m}$	Microsurface normal
D	Microfacet distribution function
G	Bidirectional shadowing-masking function
G_1	Monodirectional shadowing function
F	Fresnel term
f_r, f_r^m	Reflectance (BRDF) for macro and microsurface
f_s, f_s^m	Scattering (BSDF) for macro and microsurface
f_t, f_t^m	Transmittance (BTDF) for macro and microsurface
$\mathbf{h}_r$	Half-direction for reflection
$\mathbf{h}_t$	Half-direction for transmission
$\overrightarrow{\mathbf{h}_r}, \overrightarrow{\mathbf{h}_t}$	Unnormalized half vectors
ρ	Fraction of incident energy scattered in a mode
δ	Dirac delta function
$\left\| \frac{\partial a}{\partial b} \right\|$	Jacobian of the transform between a and b
η_i	Index of refraction of the media on the incident side
η_o, η_t	Index of refraction of media on the transmitted side
$p_m(\mathbf{m})$	Probability of choosing microsurface normal $\mathbf{m}$
$p_o(\mathbf{o})$	Probability of choosing scattered direction $\mathbf{o}$
$\chi^+(a)$	Equal to one if $a > 0$ and zero if $a \leq 0$
$\text{sign}(a)$	Sign function (1 if $a \geq 0$ and -1 if $a < 0$)
ξ_1, ξ_2	Uniform random numbers in $[0, 1)$

Figure 3: *Table of symbols.*

eral microfacet theory in Section 3. Appropriate expressions for the microsurface (smooth) reflection and refraction are developed in Section 4. We then give the rough surface reflection and refraction models in Section 5 and discuss choices for the microfacet distribution and related functions. Section 6 describes our measurement apparatus and compares our measurements to the fitted microfacet models. Appendix A reviews the Smith shadowing-masking approximation for arbitrary microfacet distributions.

2. Previous Work

Microfacet models were introduced to graphics by Cook and Torrance [CT82], based on earlier work from optics [TS67], to model light reflection from rough surfaces. Many variations have been proposed (e.g., [vSK98, KSK01, PK02]). Microfacet models are widely used in graphics and have proven effective in modeling many real surfaces [NDM05].

Ward [Lar92] introduced a simplified version of the Cook-Torrance model and extended it to reflections from anisotropic materials. He also introduced a method for sampling his model, and Beckmann distributions in general, but see [Wal05] for the correct sampling weights. An alternative sampling method using fitted separable approximations was proposed by Lawrence et al. [LRR04].

Schlick [Sch94] used rational approximation to create a cheaper approximation to the Cook-Torrance model including a widely adopted approximation to the Fresnel formula.

Ashikhmin and Shirley [AS00] introduced an anisotropic reflection model using a Phong microfacet distribution including correct importance sampling. [APS00] created energy-conserving reflection models from arbitrary microfacet distributions, though this formulation involves numerically estimating integrals without closed form solutions.

The closest work to ours is Stam [Sta01], who derived a microfacet model for refraction as part of his layered model for the reflectance of skin, and also derived the Jacobian for refraction. Unlike the present work, however, Stam did not provide importance sampling or verify his model against experimental data. He also omitted the shadowing-masking term and used a non-standard Beckmann distribution variant.

Many approximations for the shadowing-masking term have been proposed (e.g., [TS67, San69, APS00]). We use an approximation due to Smith [Smi67], which was originally derived for gaussian surfaces and later generalized [Bro80, BBS02] for arbitrary microfacet distributions.

Wave optics based reflection models have been proposed (e.g., [HTSG91]) that can simulate a wider range of surface effects than microfacet models, but they are much more expensive to evaluate and lack good importance sampling.

Numerical simulations of transmission for various rough surface models have also been performed and compared to measured results [RE75, Ger03, SN91, NSSD90].

Notation. In this work we will use boldface lowercase letters (e.g., $\mathbf{i}$ or $\mathbf{v}$) to denote unit vectors or directions. Unnormalized vectors will be written with an arrow (e.g., $\overrightarrow{\mathbf{h}}$) to clearly distinguish them. Sometimes we will describe directions using spherical polar coordinates (e.g., $\mathbf{v} = \langle \theta_v, \phi_v \rangle$). The polar angle θ will always the angle between the direction and the macrosurface normal $\mathbf{n}$, while the azimuthal angle ϕ is from some canonical direction perpendicular to $\mathbf{n}$ (which can be chosen arbitrarily for the isotropic cases we discuss). Although we describe the BSDF in terms of radiance (i.e. light
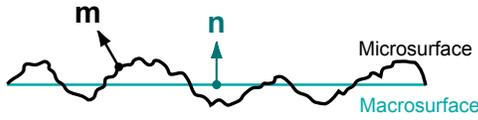
Figure 4: *Micro vs. macro surface.*

Figure 5: *Shadowing-masking geometry: Three points with the same microsurface normal* **m***. Two are visible in both the* **i** *and* **o** *directions, while one is blocked (in* **i** *in this case). By convention, we always use directions which point away from the surface.*

flow), the equations are identical when handling its dual, importance (i.e. tracing from cameras [Vea96]).

3. Microfacet Theory

A BSDF (Bidirectional Scattering Distribution Function) describes how light scatters from a surface. It is defined as the ratio of scattered radiance in a direction **o** caused per unit irradiance incident from direction **i**, and we will denote it as $f_s(\mathbf{i}, \mathbf{o}, \mathbf{n})$ to emphasize its dependence on the local surface normal **n**. If restricted to only reflection or transmission, it is often called the BRDF or BTDF, respectively, and our BSDF will be the sum of a BRDF, f_r, and a BTDF, f_t, term. Since we want to include both reflection and transmission, we will take care that our derivations and equations can correctly handle directions on either side of the surface.

In microfacet models, a detailed microsurface is replaced by a simplified macrosurface (see Figure 4) with a modified scattering function (BSDF) that matches the aggregate directional scattering of the microsurface (i.e. both should appear the same from a distance). This assumes that microsurface detail is too small to be seen directly, so only the far-field directional scattering pattern matters. Typically geometric optics is assumed and only single scattering is modeled, to simplify the problem. Wave effects and light that strikes the surface twice (or more) are ignored or must be handled separately.

Rather than working with a particular micro-surface configuration, it is assumed that the microsurface can be adequately described by two statistical measures, a microfacet distribution function D and a shadowing-masking function G, together with a microsurface BSDF f_s^m.

3.1. Microfacet Distribution Function, D

The microfacet normal distribution, $D(\mathbf{m})$, describes the statistical distribution of surface normals **m** over the microsurface. Given an infinitesimal solid angle $d\omega_m$ centered on **m**, and an infinitesimal macrosurface area dA, $D(\mathbf{m})d\omega_m dA$ is the total area of the portion of the corresponding microsurface whose normals lie within that specified solid angle. Hence D is a density function with units of 1/steradians. A plausible microfacet distribution should obey at least the following properties:

- Microfacet density is positive valued:

$$0 \le D(\mathbf{m}) \le \infty \qquad (1)$$

- Total microsurface area is at least as large as the corresponding macrosurface's area:

$$1 \le \int D(\mathbf{m})d\omega_m \qquad (2)$$

- The (signed) projected area of the microsurface is the same as the projected area of the macrosurface for any direction **v**:

$$(\mathbf{v} \cdot \mathbf{n}) = \int D(\mathbf{m})(\mathbf{v} \cdot \mathbf{m})d\omega_m \qquad (3)$$

and in the special case, $\mathbf{v} = \mathbf{n}$:

$$1 = \int D(\mathbf{m})(\mathbf{n} \cdot \mathbf{m})d\omega_m \qquad (4)$$

Equations for particular microfacet distributions are discussed in Section 5.2.

3.2. Shadowing-Masking Function, G

The bidirectional shadowing-masking function $G(\mathbf{i}, \mathbf{o}, \mathbf{m})$ describes what fraction of the microsurface with normal **m** is visible in both directions **i** and **o** (see Figure 5). Typically the shadowing-masking function has relatively little effect on the shape of the BSDF, except near grazing angles or for very rough surfaces, but is needed to maintain energy conservation. Some important properties that a plausible shadowing-masking function should obey are:

- Shadowing-masking is a fraction between zero and one:

$$0 \le G(\mathbf{i}, \mathbf{o}, \mathbf{m}) \le 1 \qquad (5)$$

- It is symmetric in the two visibility directions:

$$G(\mathbf{i}, \mathbf{o}, \mathbf{m}) = G(\mathbf{o}, \mathbf{i}, \mathbf{m}) \qquad (6)$$

- The back surface of the microsurface is never visible from directions on the front side of the macrosurface and vice-versa (sidedness agreement):

$$\begin{aligned} G(\mathbf{i}, \mathbf{o}, \mathbf{m}) = 0 \quad &\text{if} \quad (\mathbf{i} \cdot \mathbf{m})(\mathbf{i} \cdot \mathbf{n}) \le 0 \\ &\text{or} \quad (\mathbf{o} \cdot \mathbf{m})(\mathbf{o} \cdot \mathbf{n}) \le 0 \end{aligned} \qquad (7)$$

The shadowing-masking function depends on the details of the microsurface, and exact expressions are rarely available. More typically, approximations are derived using various statistical models and simplifying assumptions. See Sections 5 and Appendix A for more discussion.

3.3. Macrosurface BSDF Integral

The macrosurface BSDF is designed to match the aggregate directional (single) scattering behavior of the microsurface. We can compute it by integrating (i.e. summing) the contributions over all visible corresponding parts of the microsurface, each of which scatters light according to the microsurface's BSDF, f_s^m. The product of the D and G gives the corresponding visible area of the microsurface for each micronormal $\mathbf{m}$. We also need to apply correction factors to first transform incident irradiance onto the microsurface and then transform the scattered radiance back to the macrosurface, because both irradiance and radiance are measured relative to a surface's projected area. The resulting integral for the macrosurface BSDF is:

$$f_s(\mathbf{i}, \mathbf{o}, \mathbf{n}) = \int \left| \frac{\mathbf{i} \cdot \mathbf{m}}{\mathbf{i} \cdot \mathbf{n}} \right| f_s^m(\mathbf{i}, \mathbf{o}, \mathbf{m}) \left| \frac{\mathbf{o} \cdot \mathbf{m}}{\mathbf{o} \cdot \mathbf{n}} \right| G(\mathbf{i}, \mathbf{o}, \mathbf{m}) D(\mathbf{m}) d\omega_m \tag{8}$$

To apply this integral, we need equations for D, G, and f_s^m. We will assume that the microsurface is locally smooth so that f_s^m is a sum of terms for ideal (mirror) reflection and ideal (Snell's law) refraction, with relative strengths described by a Fresnel term F. The appropriate expressions for f_s^m will be derived in the next section.

4. Microsurface Specular BSDFs

While any BSDF could be used for the microsurface BSDF, most microfacet models assume ideal specular reflection where the microsurface acts like a collection of tiny flat mirrors (i.e. the microfacets). In this work we include both ideal reflection and ideal refraction terms.

A generic specular BSDF scatters a fraction ρ of the incident energy from direction $\mathbf{i}$ into a single specular direction $\mathbf{s}$, (where ρ and $\mathbf{s}$ are functions of $\mathbf{i}$ and the local surface normal). We can write such a specular BSDF as:

$$f_s^m(\mathbf{i}, \mathbf{o}, \mathbf{m}) = \rho \frac{\delta_{\omega_o}(\mathbf{s}, \mathbf{o})}{|\mathbf{o} \cdot \mathbf{m}|} \tag{9}$$

where $\delta_{\omega_o}(\mathbf{s}, \mathbf{o})$ is a Dirac delta function whose value is infinite when $\mathbf{s} = \mathbf{o}$ and zero otherwise. Mathematically delta functions are not functions, but rather generalized functions. They always have an associated measure (e.g., $d\omega_o$, the solid angle measure for $\mathbf{o}$) and are defined by their integral with respect to this measure:

$$\int_\Omega g(\mathbf{o}) \delta_{\omega_o}(\mathbf{s}, \mathbf{o}) d\omega_o = \begin{cases} g(\mathbf{s}) & \text{if } \mathbf{s} \in \Omega \\ 0 & \text{otherwise} \end{cases} \tag{10}$$

for any function $g()$.

To use such a BSDF in Equation 8, we need to express it in terms of microsurface normals and their associated solid angle measure. Let us assume that for any given incident and outgoing directions, there is at most one microsurface normal that scatters energy from $\mathbf{i}$ to $\mathbf{o}$, and that we can com-

pute that normal as $\mathbf{h}(\mathbf{i}, \mathbf{o})$, which we call the half-direction[†]. We can then rewrite the BSDF in terms of a delta function between $\mathbf{h}$ and $\mathbf{m}$. However, because a delta function is defined with respect to an integral, changing its associated measure requires an appropriate correction factor to preserve the value of the integral. Using the change of variables theorem, the equivalent of Equation 9 is:

$$f_s^m(\mathbf{i}, \mathbf{o}, \mathbf{m}) = \rho(\mathbf{i}, \mathbf{m}) \frac{\delta_{\omega_m}(\mathbf{h}(\mathbf{i}, \mathbf{o}), \mathbf{m})}{|\mathbf{o} \cdot \mathbf{m}|} \left\| \frac{\partial \omega_\mathbf{h}}{\partial \omega_\mathbf{o}} \right\| \tag{11}$$

where $\left\| \frac{\partial \omega_\mathbf{h}}{\partial \omega_\mathbf{o}} \right\|$ is the absolute value of the determinant of the Jacobian matrix for the transform between $\mathbf{h}$ and $\mathbf{o}$ (using solid angle measures). For brevity, the latter is often simply called the Jacobian.

The Jacobian describes the magnitude relationship between small perturbations in the two spaces. We can compute it by creating a small perturbation in the solid angle of $\mathbf{o}$, which we will denote as $d\omega_o$, and finding the induced solid angle perturbation in $\mathbf{h}$, which we will denote as $d\omega_h$ The Jacobian is defined as:

$$\left\| \frac{\partial \omega_\mathbf{h}}{\partial \omega_\mathbf{o}} \right\| = \lim_{d\omega_o \to 0} \frac{d\omega_h}{d\omega_o} \tag{12}$$

in the limit of infinitesimal perturbations. Solid angle corresponds directly to area on a unit sphere and such infinitesimal areas can be treated as approximately planar. This allows us to compute the reflection and refraction Jacobians geometrically in Figures 6 and 7. We create an infinitesimal solid angle perturbation $d\omega_o$ around $\mathbf{o}$ which is equivalent to an infinitesimal area on the unit sphere about the base of $\mathbf{o}$. We then project this area onto the the unit sphere about the base of $\mathbf{h}$ which is then equivalent to the induced solid angle perturbation $d\omega_h$ about $\mathbf{h}$, and the ratio between these infinitesimal solid angles is equal to the Jacobian. The Jacobians can also be computed algebraically from the equations relating $\mathbf{h}$ and $\mathbf{o}$ as in [Sta01].

4.1. f_r^m, Ideal Reflection

For ideal reflection, we denote the half-direction as $\mathbf{h}_r$ and its unnormalized version, the half-vector, as $\overrightarrow{\mathbf{h}_r}$ (we will use $\mathbf{h}_t$ for the transmission case). We use the standard formula for $\overrightarrow{\mathbf{h}_r}$, except that we modulate it by the sign of $(\mathbf{i} \cdot \mathbf{n})$ so that our equations will work for directions on either side of the surface (i.e. front or back). The reflection half-direction lies midway between $\mathbf{i}$ and $\mathbf{o}$, and it and its Jacobian are:

$$\mathbf{h}_r = \mathbf{h}_r(\mathbf{i}, \mathbf{o}) = \frac{\overrightarrow{\mathbf{h}_r}}{\|\overrightarrow{\mathbf{h}_r}\|} \quad \text{where} \quad \overrightarrow{\mathbf{h}_r} = \text{sign}(\mathbf{i} \cdot \mathbf{n})(\mathbf{i} + \mathbf{o}) \tag{13}$$

$$\left\| \frac{\partial \omega_{\mathbf{h}_r}}{\partial \omega_\mathbf{o}} \right\| = \frac{|\mathbf{o} \cdot \mathbf{h}_r|}{\|\overrightarrow{\mathbf{h}_r}\|^2} = \frac{1}{4|\mathbf{o} \cdot \mathbf{h}_r|} \tag{14}$$

[†] The name comes from reflection where $\mathbf{h}$ is the direction halfway in between $\mathbf{i}$ and $\mathbf{o}$, but its definition is different for refraction.
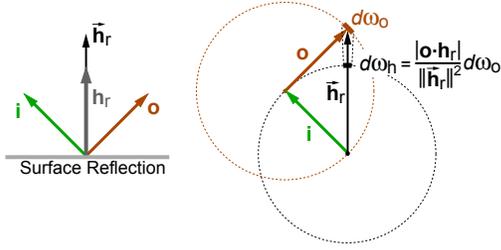
Figure 6: *Geometry for ideal reflection with half-vector* $\overrightarrow{\mathbf{h_r}} = \mathbf{i} + \mathbf{o}$ *and normalized half-direction* $\mathbf{h_r} = \overrightarrow{\mathbf{h_r}}/\|\overrightarrow{\mathbf{h_r}}\|$. *To compute the Jacobian we compute the solid angle perturbation in the normalized half vector, $d\omega_h$, induced by an infinitesimal solid angle perturbation, $d\omega_o$, in* $\mathbf{o}$. *Solid angle is directly proportional to area on the corresponding unit spheres. Only the 2D incidence plane slice through the full 3D space is shown.*

A geometric derivation of the Jacobian is illustrated in Figure 6. We have also used the facts that $\|\overrightarrow{\mathbf{h_r}}\| = (\overrightarrow{\mathbf{h_r}} \cdot \mathbf{h_r})$ and $(\mathbf{o} \cdot \mathbf{h_r}) = (\mathbf{i} \cdot \mathbf{h_r})$. The half-direction is undefined when $\mathbf{i} = -\mathbf{o}$, which is never a valid reflection configuration. For reflection we set ρ equal to the Fresnel factor F (see Section 5.1). Using Equation 11, the reflection microsurface BRDF is:

$$f_r^m(\mathbf{i},\mathbf{o},\mathbf{m}) = F(\mathbf{i},\mathbf{m}) \frac{\delta_{\omega_m}(\mathbf{h_r},\mathbf{m})}{4(\mathbf{i} \cdot \mathbf{h_r})^2} \quad (15)$$

for reflection from either side of the surface. Due to the Jacobian term, f_r^m increases as $|\mathbf{i} \cdot \mathbf{h_r}|$ decreases, and this is a principal cause of the off-specular reflection peaks predicted by microfacet models and observed in real surfaces.

4.2. f_t^m, Ideal Refraction

In the case of transmission we need the indices of refraction on either side of the surface. Let us denote the indices as η_i and η_o for the incident and transmitted sides of the surface, respectively. Ideal refraction then follows Snell's law for finding the refracted direction $\mathbf{o}$ corresponding to any incident direction $\mathbf{i}$. Snell's law can also be expressed using a half-direction $\mathbf{h_t}$ defined as:

$$\mathbf{h_t} = \mathbf{h_t}(\mathbf{i},\mathbf{o}) = \frac{\overrightarrow{\mathbf{h_t}}}{\|\overrightarrow{\mathbf{h_t}}\|} \quad \text{where} \quad \overrightarrow{\mathbf{h_t}} = -(\eta_i \mathbf{i} + \eta_o \mathbf{o}) \quad (16)$$

The magnitudes of the components of $\mathbf{i}$ and $\mathbf{o}$ perpendicular to $\mathbf{m}$ are equal to the sin of the angles between them and $\mathbf{m}$. For refraction directions, by Snell's law, these components will exactly cancel in $\mathbf{h_t}$, and the resulting direction will be colinear with $\mathbf{m}$. If we exclude the cases where $\mathbf{i}$ and $\mathbf{o}$ lie on the same side of the surface, then we will have $\mathbf{h_t} = \mathbf{m}$ if and only if $\mathbf{i}$ and $\mathbf{o}$ obey Snell's law for refraction when using $\mathbf{m}$ as the surface normal. The negative sign in $\overrightarrow{\mathbf{h_t}}$ is because we use the convention that surface normals point into the medium with the lower index of refraction (e.g., air). We assume that the two sides of the surface have different
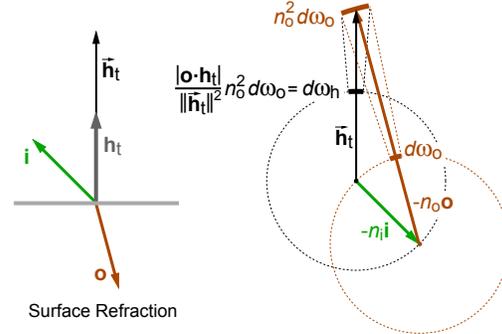
Figure 7: *Geometry for ideal refraction with half-vector* $\overrightarrow{\mathbf{h_t}} = -\eta_i \mathbf{i} - \eta_o \mathbf{o}$ *and normalized half-direction* $\mathbf{h_t} = \overrightarrow{\mathbf{h_t}}/\|\overrightarrow{\mathbf{h_t}}\|$. *We compute the Jacobian by taking a infinitesimal solid angle perturbation $d\omega_o$ in $\mathbf{o}$, projecting into a perturbation in $\overrightarrow{\mathbf{h_t}}$ and then onto the unit sphere for $\mathbf{h_t}$. Only the 2D incidence plane slice through the full 3D space is shown.*

indices of refraction; otherwise $\mathbf{h_t}$ becomes ill-defined. The corresponding Jacobian (see Figure 7) is:

$$\left\| \frac{\partial \omega_{\mathbf{h_t}}}{\partial \omega_{\mathbf{o}}} \right\| = \frac{\eta_o^2 |\mathbf{o} \cdot \mathbf{h_t}|}{\|\overrightarrow{\mathbf{h_t}}\|^2} = \frac{\eta_o^2 |\mathbf{o} \cdot \mathbf{h_t}|}{(\eta_i(\mathbf{i} \cdot \mathbf{h_t}) + \eta_o(\mathbf{o} \cdot \mathbf{h_t}))^2} \quad (17)$$

We assume no light is absorbed at the interface so the ρ for refraction is one minus the fresnel factor F. Using Equation 11, we can write the microsurface refraction BSDF as:

$$f_t^m(\mathbf{i},\mathbf{o},\mathbf{m}) = (1 - F(\mathbf{i},\mathbf{m})) \frac{\delta_{\omega_m}(\mathbf{h_t},\mathbf{m}) \eta_o^2}{(\eta_i(\mathbf{i} \cdot \mathbf{h_t}) + \eta_o(\mathbf{o} \cdot \mathbf{h_t}))^2} \quad (18)$$

Note that this BTDF does not obey reciprocity, instead we have $f_t^m(\mathbf{i},\mathbf{o},\mathbf{m})/\eta_o^2 = f_t^m(\mathbf{o},\mathbf{i},\mathbf{m})/\eta_i^2$. This is a well-known property of refractive interfaces [Vea96][‡] and if desired we can restore reciprocity by tracking radiance/η^2 instead of radiance (sometimes called basic radiance). As in reflectance, the BTDF increases towards grazing angles due to the Jacobian term which similarly causes off-specular peaks in the refracted lobe.

5. BSDF for Rough Surfaces

Using the microsurface BSDFs for reflection and refraction together with Equation 8, we can now write the equation for the macrosurface reflection and refraction BSDF f_s, which is sum of BRDF and BTDF terms:

$$f_s(\mathbf{i},\mathbf{o},\mathbf{m}) = f_r(\mathbf{i},\mathbf{o},\mathbf{m}) + f_t(\mathbf{i},\mathbf{o},\mathbf{m}) \quad (19)$$

The reflection term is:

$$f_r(\mathbf{i},\mathbf{o},\mathbf{n}) = \frac{F(\mathbf{i},\mathbf{h_r}) \, G(\mathbf{i},\mathbf{o},\mathbf{h_r}) \, D(\mathbf{h_r})}{4 \, |\mathbf{i} \cdot \mathbf{n}| \, |\mathbf{o} \cdot \mathbf{n}|} \quad (20)$$

[‡] While Veach correctly points out that refractive BTDFs are not reciprocal, he incorrectly claims they are not self-adjoint. In fact the equations are same whether transporting radiance (from lights) or importance (from cameras).

This is exactly the same as the Cook-Torrance BSDF except that we have a factor of 4 in the denominator instead of π. However, the original paper used a different normalization for D. Other more recent papers agree with our constant of four (e.g., [Sta01]).

The corresponding refraction term is:

$$f_t(\mathbf{i}, \mathbf{o}, \mathbf{n}) = \frac{|\mathbf{i} \cdot \mathbf{h}_t| \, |\mathbf{o} \cdot \mathbf{h}_t|}{|\mathbf{i} \cdot \mathbf{n}| \, |\mathbf{o} \cdot \mathbf{n}|} \frac{\eta_o^2 \, (1 - F(\mathbf{i}, \mathbf{h}_t)) \, G(\mathbf{i}, \mathbf{o}, \mathbf{h}_t) \, D(\mathbf{h}_t)}{(\eta_i (\mathbf{i} \cdot \mathbf{h}_t) + \eta_o (\mathbf{o} \cdot \mathbf{h}_t))^2} \tag{21}$$

We don't get as much nice cancellation of terms in the refraction component, but it is still easily implemented and evaluated. This completes our derivation of the basic BSDF equations for the microfacet model of reflection and transmission through rough dielectric surfaces.

5.1. Choosing F, D, and G

Using Equations 20 and 21, requires appropriate choices for the F, D, and G, terms. The Fresnel term is the best understood, and exact equations are available in the literature. The Fresnel term is typically small at normal incidence (e.g., 0.04 for glass with $\eta_t = 1.5$) and increases to unity at grazing angles or for total internal reflection. A convenient exact formulation for dielectrics with unpolarized light is [CT82]:

$$F(\mathbf{i}, \mathbf{m}) = \frac{1}{2} \frac{(g-c)^2}{(g+c)^2} \left(1 + \frac{(c(g+c)-1)^2}{(c(g-c)+1)^2} \right) \tag{22}$$

$$\text{where } g = \sqrt{\frac{\eta_t^2}{\eta_i^2} - 1 + c^2} \text{ and } c = |\mathbf{i} \cdot \mathbf{m}|$$

Note that if g is imaginary, this indicates total internal reflection and $F = 1$ in this case. Cheaper approximations for F are also sometimes used [CT82, Sch94].

A wide variety of microfacet distribution functions D have been proposed. In this paper, we discuss three different types: Beckmann, Phong, and GGX. The Beckmann distribution arises from Gaussian roughness assumptions for the microsurface and is widely used in the optics literature. The Phong distribution is a purely empirical one developed in the graphics literature; however, with suitable choices of width parameters it is very similar to the Beckmann distribution. The GGX distribution is new, and we developed it to better match our measured data for transmission. Equations for the three distribution types and related functions are given at the end of this section.

The shadowing-masking term G depends on the distribution function D and the details of the microsurface, so exact solutions are rarely possible. Cook & Torrance used a G based on a 1D model of parallel grooves that guarantees energy conservation for any distribution D, but we do not recommend using it because it contains first derivative discontinuities and other features not seen in real surfaces. Instead we will use the Smith shadowing-masking approximation [Smi67]. The Smith G was originally derived for Gaussian
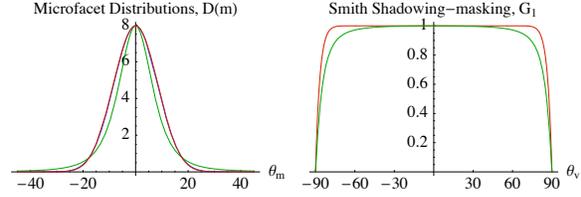
Figure 8: *Left: Beckmann (red), Phong (blue), and GGX (green) distribution functions $D(\mathbf{m})$ with $\alpha_b = 0.2$, $\alpha_p = 48$, and $\alpha_g = 0.2$ respectively. Beckmann and Phong are nearly identical while GGX has a narrower peak with stronger tails. Right: Smith shadowing-masking term $G_1(\mathbf{v}, \mathbf{n})$ for same Beckmann (red) and GGX (green) distributions. G_1 is near one except at grazing angles and GGX has more shadowing due to its stronger tails.*

rough surfaces, but has since been extended to handle surfaces with arbitrary distribution functions [Bro80, BBS02], though in some cases (e.g., Phong), the resulting integrals have no simple closed form solution.

The Smith G approximates the bidirectional shadowing-masking as the separable product of two monodirectional shadowing terms G_1:

$$G(\mathbf{i}, \mathbf{o}, \mathbf{m}) \approx G_1(\mathbf{i}, \mathbf{m}) G_1(\mathbf{o}, \mathbf{m}) \tag{23}$$

where G_1 is derived from the microfacet distribution D as described in [Smi67, Bro80, BBS02] and Appendix A. Smith actually derived two different shadowing functions: one when the microsurface normal $\mathbf{m}$ is known, and another averaged over all microsurface normals. Although the latter is more frequently used in the literature (e.g., [HTSG91]), in microfacet models, where we know the microsurface normal of interest, the former is more appropriate and we use it in this paper.

5.2. Specific Distributions and Related Functions

Below we give the equations for the Beckmann, Phong, and GGX distributions D (see Figure 8), along with their associated Smith shadowing functions G_1, and sampling equations to generate microsurface normals from two uniform random variables ξ_1 and ξ_2 in the interval $[0, 1)$. The probability of generating any $\mathbf{m}$ using the given sampling equations is:

$$p_m(\mathbf{m}) = D(\mathbf{m}) |\mathbf{m} \cdot \mathbf{n}| \tag{24}$$

Note that θ_m is the angle between $\mathbf{m}$ and $\mathbf{n}$, θ_v between $\mathbf{v}$ and $\mathbf{n}$, and $\chi^+(a)$ is the positive characteristic function (which equals one if $a > 0$ and zero if $a \leq 0$). These are all heightfield distributions (i.e. $D(\mathbf{m}) = 0$ if $\mathbf{m} \cdot \mathbf{n} \leq 0$), and anisotropic variants exist but will not be discussed here.

Beckmann Distribution with width parameter α_b:

$$D(\mathbf{m}) = \frac{\chi^+(\mathbf{m} \cdot \mathbf{n})}{\pi \alpha_b^2 \cos^4 \theta_m} \, e^{\frac{-\tan^2 \theta_m}{\alpha_b^2}} \tag{25}$$

$$G_1(\mathbf{v}, \mathbf{m}) \;=\; \chi^+\!\left(\frac{\mathbf{v}\cdot\mathbf{m}}{\mathbf{v}\cdot\mathbf{n}}\right)\; \frac{2}{1+\mathrm{erf}(a)+\frac{1}{a\sqrt{\pi}}e^{-a^2}} \quad (26)$$

$$\text{with}\quad a = (\alpha_b \tan\theta_v)^{-1}$$

In the G_1 equation, the first factor enforces sidedness agreement (i.e. $\mathbf{v}$ must be on same side of the macro and microsurfaces). Because it involves the error function, $\mathrm{erf}(x) = \frac{2}{\sqrt{\pi}}\int_0^x e^{-x^2}\,dx$, this equation can be expensive to evaluate. Schlick [Sch94] proposed using a cheaper rational approximation, but based it on a different shadowing-masking equation. Instead, we provide the following rational approximation to the Smith G_1 equation above with relative error of less than 0.35%.

$$G_1(\mathbf{v}, \mathbf{m}) \approx \chi^+\!\left(\frac{\mathbf{v}\cdot\mathbf{m}}{\mathbf{v}\cdot\mathbf{n}}\right) \begin{cases} \dfrac{3.535a+2.181a^2}{1+2.276a+2.577a^2} & \text{if } a < 1.6 \\[2ex] 1 & \text{otherwise} \end{cases} \quad (27)$$

The equations for sampling $D(\mathbf{m})\,|\mathbf{m}\cdot\mathbf{n}|$ are:

$$\theta_m \;=\; \arctan\sqrt{-\alpha_b^2 \log(1-\xi_1)} \quad (28)$$

$$\phi_m \;=\; 2\pi\xi_2 \quad (29)$$

Phong Distribution with exponent parameter α_p:

$$D(\mathbf{m}) = \chi^+(\mathbf{m}\cdot\mathbf{n})\,\frac{\alpha_p+2}{2\pi}\,(\cos\theta_m)^{\alpha_p} \quad (30)$$

Note that if we set $\alpha_p = 2\alpha_b^{-2}-2$, then the Phong and Beckmann distributions are very similar, especially for narrow widths (see Figure 8), and this may help explain the longevity of the purely empirical Phong distribution. In graphics applications, it is reasonable to choose between them based on computational convenience. Unfortunately the integrals to compute the Smith G_1 have no closed form solution for the Phong distribution. Based on its similarity to Beckmann and some numerical testing, we recommend instead using Equation 27 with $a = \sqrt{0.5\alpha_p+1}/(\tan\theta_v)$ for the G_1 term for Phong. The equations for sampling $D(\mathbf{m})\,|\mathbf{m}\cdot\mathbf{n}|$ are:

$$\theta_m \;=\; \arccos\left(\xi_1^{\frac{1}{\alpha_p+2}}\right) \quad (31)$$

$$\phi_m \;=\; 2\pi\xi_2 \quad (32)$$

GGX Distribution with width parameter α_g:

$$D(\mathbf{m}) = \frac{\alpha_g^2\,\chi^+(\mathbf{m}\cdot\mathbf{n})}{\pi\cos^4\theta_m\,(\alpha_g^2+\tan^2\theta_m)^2} \quad (33)$$

$$G_1(\mathbf{v},\mathbf{m}) = \chi^+\!\left(\frac{\mathbf{v}\cdot\mathbf{m}}{\mathbf{v}\cdot\mathbf{n}}\right)\frac{2}{1+\sqrt{1+\alpha_g^2\tan^2\theta_v}} \quad (34)$$

The GGX distribution has stronger tails than the Beckmann

and Phong distributions and thus tends to have more shadowing. The equations for sampling $D(\mathbf{m})\,|\mathbf{m}\cdot\mathbf{n}|$ are:

$$\theta_m \;=\; \arctan\left(\frac{\alpha_g\sqrt{\xi_1}}{\sqrt{1-\xi_1}}\right) \quad (35)$$

$$\phi_m \;=\; 2\pi\xi_2 \quad (36)$$

5.3. Sampling and Weights

To sample the BSDF, we assume that we are given a direction $\mathbf{i}$ and we want to generate scattered directions $\mathbf{o}$ in a pattern that closely matches $f_s(\mathbf{i}, \mathbf{o}, \mathbf{n})\,|\mathbf{o}\cdot\mathbf{n}|$. In general, a microfacet BSDF cannot be sampled exactly. Our approach will be to first sample a microsurface normal $\mathbf{m}$, and then use it to generate scattered directions $\mathbf{o}$. To compute the weights for the corresponding samples, we also need to compute the probability density p_o of the sample directions. The resulting weights will be:

$$\text{weight}(\mathbf{o}) = \frac{f_s(\mathbf{i},\mathbf{o},\mathbf{n})\,|\mathbf{o}\cdot\mathbf{n}|}{p_o(\mathbf{o})} \quad (37)$$

where we want to choose the sampling to minimize the variance in the resulting weights.

If we choose the microfacet normal $\mathbf{m}$ with some probability p_m and invert the half-direction formulas (i.e. Equation 13 or 16) to generate the corresponding scattered direction $\mathbf{o}$, then the resulting probability will include the Jacobian of the half-direction transform (e.g., see [Wal05]):

$$p_o(\mathbf{o}) = p_m(\mathbf{m})\left\|\frac{\partial\omega_h}{\partial\omega_o}\right\| \quad (38)$$

Using the sampling equations from Section 5.2, we can generate sampled microfacet normals $\mathbf{m}$ according to the probability $p_m(\mathbf{m}) = D(\mathbf{m})\,|\mathbf{m}\cdot\mathbf{n}|$. We can then evaluate the Fresnel term $F(\mathbf{i},\mathbf{m})$ and use it to select between reflection and refraction, thus also folding the Fresnel term into the probability. For reflection, the scattered direction $\mathbf{o}_r$ is:

$$\mathbf{o}_r \;=\; 2\,|\mathbf{i}\cdot\mathbf{m}|\,\mathbf{m}\,-\,\mathbf{i} \quad (39)$$

and for transmission the scattered direction $\mathbf{o}_t$ is:

$$\mathbf{o}_t = \left(\eta\,c - \mathrm{sign}(\mathbf{i}\cdot\mathbf{n})\sqrt{1+\eta(c^2-1)}\right)\mathbf{m} - \eta\,\mathbf{i}$$

$$\text{with}\quad c = (\mathbf{i}\cdot\mathbf{m}) \quad\text{and}\quad \eta = \eta_i/\eta_t \quad (40)$$

And in either case the resulting weight for the scattered direction is:

$$\text{weight}(\mathbf{o}) = \frac{f_s(\mathbf{i},\mathbf{o},\mathbf{n})\,|\mathbf{o}\cdot\mathbf{n}|}{p_o(\mathbf{o})} = \frac{|\mathbf{i}\cdot\mathbf{m}|\,G(\mathbf{i},\mathbf{o},\mathbf{m})}{|\mathbf{i}\cdot\mathbf{n}|\,|\mathbf{m}\cdot\mathbf{n}|} \quad (41)$$

At normal incidence (i.e. $|\mathbf{i}\cdot\mathbf{n}| \approx 1$) this is a nearly perfect sampling. At grazing angles, it is still a good sampling but it is possible to produce sample weights as high as hundreds to millions depending on the choices and parameters for D and G. While such high weights are unlikely (worst for retroreflection at grazing where f_s is very small), they can cause
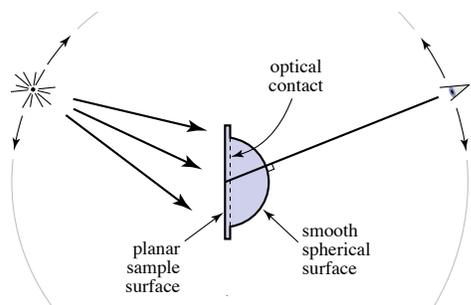
Figure 9: *Measurement setup: We bonded a glass hemisphere to the back of our samples, to allow us to observe transmission even at grazing angles.*

problems for methods that assume such high weights never occur (e.g., most particle tracing methods). We can greatly reduce the maximum weight by modifying the sampling distribution slightly. For example, with the Beckmann distribution, we can instead sample a slightly widened distribution given by $\alpha_b^\dagger = (1.2 - 0.2\sqrt{|\mathbf{i} \cdot \mathbf{n}|})\alpha_b$. This reduces the maximum sample weight to roughly four, a significant reduction.

6. Measurements

In order to validate our scattering model, we made measurements of transmission through several different types of rough glass surfaces. This measurement cannot be made simply by illuminating a plate of rough-surfaced glass and measuring the scattered light, because the light cannot be directly observed inside the glass, and internal reflection will prevent light that scatters into relatively grazing directions from escaping to where it can be measured. At the same time, the large amount of internally reflected light will re-illuminate the rough surface from the inside, producing an unacceptable amount of stray light.

In order to directly observe the transmitted light, we eliminate the second interface by cementing a plano-convex lens that is nearly a hemisphere to the back of the sample (Figure 9). This configuration was inspired by the work of [NN04]. The sample is illuminated from the rough surface and viewed from a range of angles through the spherical surface, with the center of rotation of the apparatus aligned with the center of the spherical surface so that the view direction is always perpendicular to the surface. This way, the scattered light exits the surface with minimal loss due to Fresnel reflection. Also, relatively little light is reflected back onto the area near the center of the sample, since the reflection paths off the hemisphere are nearly perpendicular to the surface. This greatly reduces the stray-light problem compared with a flat sample.

In our setup, a 100mm square sample is cemented using index-matched adhesive[§] to a 75mm diameter, 75mm focal

length plano-convex lens, which is nearly a hemisphere. For samples of about 6mm thickness, the center of the lens's spherical surface is on the rough surface. However, our samples are of varying thickness, so the method must tolerate a distance of a few mm between the surface and the center.

The sample is illuminated from the rough side by the end of a 6mm circular fiber optic light guide at a distance of 610 mm (illumination solid angle: .000076 sr). The light source was a DC regulated fiber illuminator, providing stable and flicker-free illumination over the entire sample surface. The transmitted light was sensed by a cooled CCD camera viewing the sample from the hemispherical side from a distance of 885 mm through a 35mm imaging lens at f/5.6 (receiving solid angle: .000039 sr). The measurement was made by averaging the pixel values in a fixed rectangle in the camera image corresponding to an area on the spherical surface up to approximately 3mm x 10mm.[¶]

Because the measured area is defined by a fixed area in the image, the measurements are proportional to the radiance observed by the camera. Since radiance is preserved (up to a constant factor) under refraction, this arrangement produces a signal proportional to the BTDF times the cosine of the incident angle. It is important to illuminate from the front and view from the back to have this property; if the sample was flood-illuminated from the hemispherical side, the lens would focus the light into a nonuniform distribution of irradiance that would make the system sensitive to exact alignment between the sphere center and the surface.

We measured four samples of glass with rough surfaces generated by different processes. One was commercially produced ground glass created by sandblasting soda-lime glass with 120 abrasive (*ground*, 1/16 inch thickness). One sample was prepared in our lab by acid-etching one side of a plate of soda-lime glass (*etched*, 3/16 inch thickness). The last two are less well characterized: commercially available frosted glass (*frosted*, 1/8 inch thickness) and commercially available antiglare glass for picture framing (*antiglare*, 1/16 inch thickness). All samples had flat polished surfaces on the reverse side except the antiglare glass, which was rough on both sides; we assume that the adhesive fills in the surface so that the extra rough interface is not relevant (and in fact, there is no visible evidence of an air layer).

The measurements consistently show a clear shift in the peak of the scattered lobe away from the expected refraction direction. When the roughness is low, as in the antiglare glass, the peak is near the ideal refraction angle, but for the rougher samples it is substantially shifted toward grazing.

[§] All the samples are soda-lime glass (the commercial samples are

assumed to be), with refractive index around 1.51. The spherical lenses are BK7 optical glass, with refractive index 1.52, and the cured adhesive has specified refractive index 1.50. The slight difference in index creates only negligible reflection over the range of angles we measured.

[¶] Smaller areas were used for less-diffusing samples, in order to ensure the signal was relatively constant over the measured area.
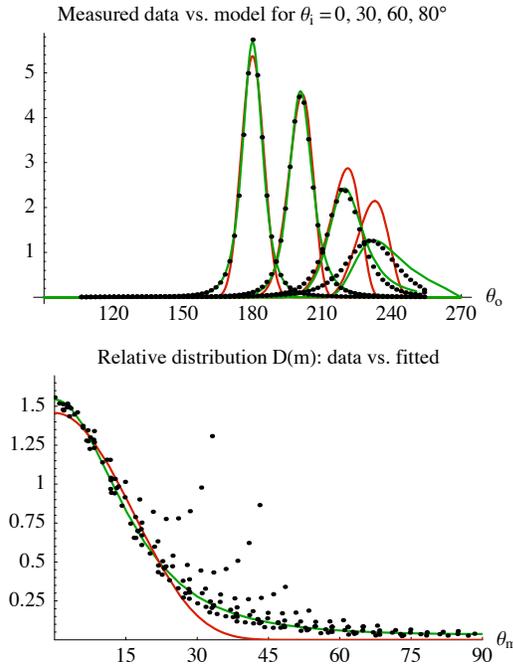
Figure 10: *Ground glass sample. Top is BTDF fit and bottom is the fit to the empirical microfacet distribution D. Red line is Beckmann fit and green is GGX fit.*
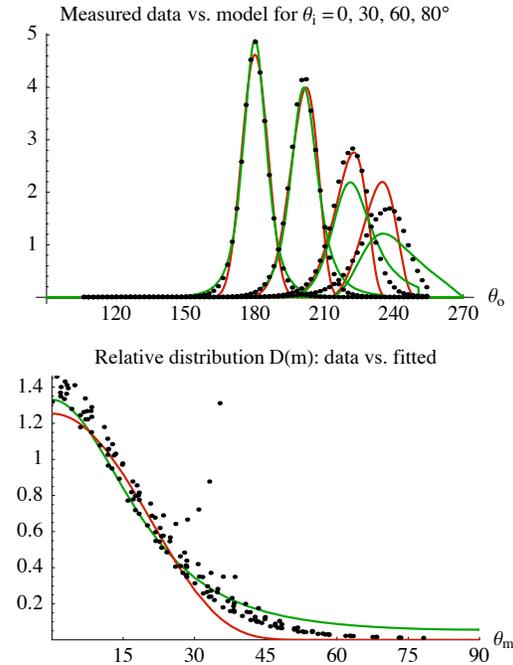
Figure 11: *Frosted sample. Top is BTDF fit and bottom is the fit to the empirical microfacet distribution D. Red line is Beckmann fit and green is GGX fit.*

For this reason many of the features of these rough-surface BTDFs are difficult to observe directly in a flat plate. As we show next, our microfacet models predict this behavior well.

6.1. Sample Results

For each of our four samples we fitted our microfacet BTDF to our measured transmission data for normal incidence using both the Beckmann and GGX distributions (see Figure 12). For all samples we assumed an index of refraction of 1.51. This gives us two free parameters to fit: the distribution width parameter (α_b or α_g) and an overall scaling factor to map our measurements to an absolute scale.

To test our BTDF model, we show two plots for each sample. The first shows $f_t(\mathbf{i}, \mathbf{o}, \mathbf{n}) |\mathbf{o} \cdot \mathbf{n}|$ as a function of the transmitted angle θ_o. We show both the normal incidence case ($\theta_i = 0$), where we performed the fitting, and three additional incidence angles ($\theta_i = 30, 60, 80°$) to test the models ability to extrapolate to these angles.

The second plot directly estimates points in the microfacet distribution function D from the data. Since the G term is close to one except at grazing angles, if we only use data points far from grazing (i.e. where $|\mathbf{i} \cdot \mathbf{n}| > 0.5$ and $|\mathbf{o} \cdot \mathbf{n}| > 0.5$, and assume $G(\mathbf{i}, \mathbf{o}, \mathbf{m}) = 1$ for these points, we can solve Equation 21 for the corresponding values of $D(\mathbf{h}_t)$. We also excluded points with very low measured values as

these are easily affected by stray light. If the data fits a microfacet model, then these points should all lie close to a curve which is the surface's microfacet distribution function. Note that in both plots the models have been scaled by the fitted scaling factors to enable comparison with the relative measured data.

The data and model fits for the ground glass sample are shown in Figure 10. We can see that the GGX distribution provides an excellent fit to the data and is much closer than the Beckmann fit. The only significant differences occur at near-grazing angles where the microfacet assumptions of geometric optics and single scattering may be less valid. We

Sample	Beckmann Fit		GGX Fit	
	scale	α_b	scale	α_g
ground	0.542	0.344	0.755	0.394
frosted	0.629	0.400	0.861	0.454
etched	0.711	0.493	0.955	0.553
antiglare	0.607	0.023	0.847	0.027

Figure 12: *Fitted coefficients for our four samples. We fitted the measured data for normal incidence to our BTDF using both the Beckmann and GGX microfacet distributions. In each case we fit both the distribution width parameter and an overall scaling factor (because we have relative rather than absolute measurements).*

Measured data vs. model for $\theta_i = 0, 30, 60, 80°$

Relative distribution D(m): data vs. fitted
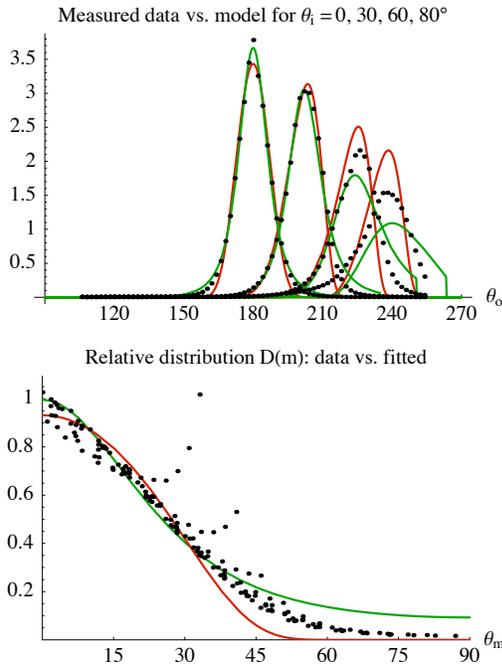
Figure 13: *Etched sample. Top is BTDF fit and bottom is the fit to the empirical microfacet distribution D. Red line is Beckmann fit and green is GGX fit.*

Measured data vs. model for $\theta_i = 0, 30, 60, 80°$

Relative distribution D(m): data vs. fitted

Figure 14: *Antiglare sample. Top is BTDF fit and bottom is the fit to the empirical microfacet distribution D. Red line is Beckmann fit and green is GGX fit.*

developed the GGX distribution specifically to fit this sample after we discovered that the Beckmann distribution did not match the inferred microfacet distribution as shown in the bottom plot.

The plots for the frosted glass and etched glass samples are shown in Figures 11 and 13. For both samples, both the Beckmann and GGX fits do a reasonable job of matching the measured transmission pattern, but neither is able to exactly match the empirical microfacet distribution functions as shown in the lower plots. Most likely we could get even better matches by finding distribution functions with behavior somewhere between that of Beckmann and GGX.

The antiglare glass has a much lower surface roughness than the other samples and consequently a much narrower lobe as shown in Figure 14. Because its so narrow, we get relatively few samples within the lobe and had more trouble in estimating its width. In this case both the Beckmann and GGX fits perform equally well.

Using our BTDF model and sampling techniques, we have rendered simulations of the antiglare, ground, and etched samples in Figure 15. These images do a good job of duplicating their different appearances, and their ability to obscure patterns and diffuse light. A simulation of an pattern-etched glass globe is shown in Figure 1.

7. Conclusions

In this paper, we have provided a comprehensive review of microfacet theory and shown how it can be extended to handle transmissive materials with rough surfaces. We have validated the resulting BTDF models against measured data and shown that they can predict the refraction behavior of real surfaces. We developed a new microfacet distribution function (the GGX distribution) and shown that at least for some surfaces it provides a closer match to the measured data than the standard Beckmann distribution. We have also described how to efficiently importance sample the microfacet model which is essential when rendering transmitted light. We believe these techniques can prove useful in enabling simulation of a wider range of materials including improved models of translucent materials such as skin, marble, and paint.

References

[APS00] ASHIKHMIN M., PREMOZE S., SHIRLEY P. S.: A microfacet-based BRDF generator. In *Proceedings of ACM SIGGRAPH 2000* (July 2000), pp. 65–74.

[AS00] ASHIKHMIN M., SHIRLEY P. S.: An anisotropic phong BRDF model. *Journal of Graphics Tools 5*, 2 (2000), 25–32.
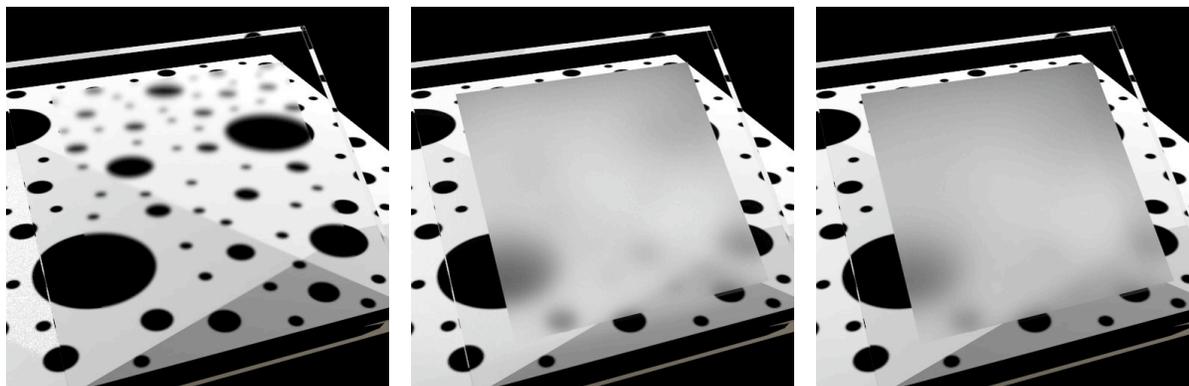
| anti-glare (Beckman, $\alpha_b = 0.023$) | ground (GGX, $\alpha_g = 0.394$) | etched (GGX, $\alpha_g = 0.553$) |

Figure 15: *Simulations of a glass slide with a rectangle of roughened surface using the fitted distributions from out anti-glare, ground, and etched glass samples.*

[BBS02] BOURLIER C., BERGINC G., SAILLARD J.: One- and two-dimensional shadowing functions for any height and slope stationary uncorrelated surface in the monostatic and bistatic configurations. *IEEE Trans. on Antennas and Propagation 50* (Mar. 2002), 312–324.

[Bro80] BROWN G. S.: Shadowing by non-Gaussian random surfaces. *IEEE Trans. on Antennas and Propagation 28* (Nov. 1980), 788–790.

[CT82] COOK R. L., TORRANCE K. E.: A reflectance model for computer graphics. *ACM Transactions on Graphics 1*, 1 (Jan. 1982), 7–24.

[Ger03] GERMER T. A.: Polarized light diffusely scattered under smooth and rough interfaces. In *Polarization Science and Remote Sensing.* (Dec. 2003), vol. 5158 of *Proceedings of the SPIE*, pp. 193–204.

[HTSG91] HE X. D., TORRANCE K. E., SILLION F. X., GREENBERG D. P.: A comprehensive physical model for light reflection. In *Computer Graphics (Proceedings of SIGGRAPH 91)* (July 1991), pp. 175–186.

[KSK01] KELEMEN C., SZIRMAY-KALOS L.: A microfacet based coupled specular-matte BRDF model with importance sampling. *Eurographics Short Presentations* (2001).

[Lar92] LARSON G. J. W.: Measuring and modeling anisotropic reflection. In *Computer Graphics (Proceedings of SIGGRAPH 92)* (July 1992), pp. 265–272.

[LRR04] LAWRENCE J., RUSINKIEWICZ S., RAMAMOORTHI R.: Efficient BRDF importance sampling using a factored representation. *ACM Transactions on Graphics 23*, 3 (Aug. 2004), 496–505.

[NDM05] NGAN A., DURAND F., MATUSIK W.: Experimental analysis of BRDF models. In *Rendering Techniques 2005: Eurographics Symposium on Rendering* (June 2005), pp. 117–126.

[NN04] NEE S.-M. F., NEE T.-W.: Polarization of transmission scattering simulated by using a multiple-facets model. *Journal of the Optical Society of America A 21* (Sept. 2004), 1635–1644.

[NSSD90] NIETO-VESPERINAS M., SANCHEZ-GIL J. A., SANT A. J., DAINTY J. C.: Light transmission from a randomly rough dielectric diffuser: theoretical and experimental results. *Optics Letters 15* (Nov. 1990), 1261–1263.

[PK02] PONT S. C., KOENDERINK J. J.: Bidirectional reflectance distribution function of specular surfaces with hemispherical pits. *Journal of the Optical Society of America A 19* (Dec. 2002), 2456–2466.

[RE75] ROGERS J. E., EDWARDS D. K.: Bidirectional reflectance and transmittance of a scattering-absorbing medium with a rough surface. In *Thermophysics Conference* (May 1975).

[San69] SANCER M. I.: Shadow Corrected Electromagnetic Scattering from Randomly Rough Surfaces. *IEEE Trans. on Antennas and Propagation 17* (1969), 577–585.

[Sch94] SCHLICK C.: An inexpensive BRDF model for physically-based rendering. *Computer Graphics Forum 13*, 3 (1994), 233–246.

[Smi67] SMITH B. G.: Geometrical shadowing of a random rough surface. *IEEE Trans. on Antennas and Propagation* (1967), 668–671.

[SN91] SÁNCHEZ-GIL J. A., NIETO-VESPERINAS M.: Light scattering from random rough dielectric surfaces. *Journal of the Optical Society of America A 8* (Aug. 1991), 1270–1286.

[Sta01] STAM J.: An illumination model for a skin layer bounded by rough surfaces. In *Rendering Techniques 2001: 12th Eurographics Workshop on Rendering* (June 2001), pp. 39–52.

[TS67] TORRANCE K. E., SPARROW E. M.: Theory for

off-specular reflection from roughened surfaces. *Journal of Optical Society of America 57*, 9 (1967), 1105–1114.

[Vea96] VEACH E.: Non-symmetric scattering in light transport algorithms. In *Eurographics Rendering Workshop 1996* (June 1996), pp. 81–90.

[vSK98] VAN GINNEKEN B., STAVRIDI M., KOENDERINK J. J.: Diffuse and Specular Reflectance from Rough Surfaces. *Applied Optics 37* (Jan. 1998), 130–139.

[Wal05] WALTER B.: *Notes on the Ward BRDF*. Technical Report PCG-05-06, Cornell Program of Computer Graphics, Apr. 2005.

Appendix A: Deriving the Smith Shadowing, G_1

This appendix briefly reviews deriving the Smith shadowing function G_1 from the microfacet distribution D; see the references for more details. Originally created for Gaussian random surfaces [Smi67], the Smith G_1 has been generalized to other microfacet distributions [Bro80, BBS02].

Let us assume we can represent the microsurface as a random heightfield relative to the macrosurface characterized by two probability distributions: $P_1(\xi)$ for height ξ, and $P_{22}(p,q)$ for the microsurface 2D slopes p and q, measured perpendicular and parallel to the incidence plane respectively. P_1 can be any probability function without changing the result. The 2D slope probability P_{22} can be computed from D using the relation:

$$P_{22}(p,q) = D(\mathbf{m}) \cos^4 \theta_m \qquad (42)$$

where the cosine factors are due to the change of measure (solid angle vs. slopes) and projection onto the macrosurface. For the Beckmann distribution, it is easily shown that (using the relation $\tan^2 \theta_m = p^2 + q^2$) P_{22} is just a standard 2D Gaussian. The 1D distribution of slopes q in the incidence plane, P_2, is:

$$P_2(q) = \int_{-\infty}^{\infty} P_{22}(p,q)\,dp \qquad (43)$$

Let $S(\xi_0,\mu)$ be the probability that a random point on the microsurface with height ξ_0 is visible from direction $\mathbf{v}$, where μ is the slope of the visibility ray (see Figure 16):

$$\mu = |\cot \theta_v| \qquad (44)$$

Parameterizing the ray by its projected distance τ on the macrosurface, the ray's height at τ is $\xi_0 + \mu\tau$. Let $g(\tau)\Delta\tau$ be the fraction of previously unoccluded rays that first intersect the microsurface in the interval $[\tau, \tau + \Delta\tau]$, so that:

$$S(\xi_0,\mu) = e^{-\int_0^{\infty} g(\tau)\,d\tau} \qquad (45)$$

where g acts similarly to the attenuation coefficient in volume rendering. To compute g, we assume that the surface height and slope distributions are independent and that g can be approximated as: what fraction of the rays that start the interval above the surface are below the surface at the end of it
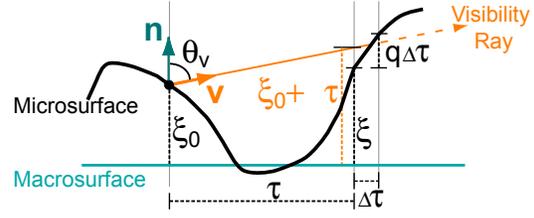
Figure 16: *Geometry for Smith shadowing-masking G_1 for direction* **v**, *corresponding to a visibility ray has starting height ξ_0 and slope μ. At distance τ (measured along macrosurface), the microsurface has height ξ and slope q.*

(and hence intersected the surface somewhere in $[\tau, \tau + \Delta\tau]$). If ξ and q are the height and slope of the surface at τ, then the ray is above the surface at τ if $\xi_0 + \mu\tau > \xi$ and below the surface at $\tau + \Delta\tau$ if $(q - \mu)\Delta\tau > (\xi_0 + \mu\tau) - \xi$. Thus we get:

$$g(\tau) = \frac{\int_{\mu}^{\infty} (q - \mu) P_1(\xi_0 + \mu\tau) P_2(q)\,dq}{\int_{-\infty}^{\xi_0 + \mu\tau} P_1(\xi)\,d\xi}$$

$$= \Lambda(\mu)\,\frac{\mu P_1(\xi_0 + \mu\tau)}{f(\xi_o + \mu\tau)} \qquad (46)$$

where $f(z)$ is the probability z is above the surface, and Λ is:

$$f(z) = \int_{-\infty}^{z} P_1(\xi)\,d\xi \qquad (47)$$

$$\Lambda(\mu) = \frac{1}{\mu}\int_{\mu}^{\infty} (q - \mu) P_2(q)\,dq \qquad (48)$$

We can solve Equation 45 by noting that the numerator in Equation 46 is the derivative of its denominator to that:

$$S(\xi_0,\mu) = e^{\Lambda(\mu)\log f(\xi_0)} = f(\xi_0)^{\Lambda(\mu)} \qquad (49)$$

and then we integrate over all starting heights ξ_0 to find $S(\mu)$, the average visibility over all starting microsurface heights:

$$S(\mu) = \int_{-\infty}^{\infty} S(\xi_0,\mu) P_1(\xi_0)\,d\xi_0 = \frac{1}{1 + \Lambda(\mu)} \qquad (50)$$

where we used the fact that the derivative of $f(\xi_0)$ is $P_1(\xi_0)$.

Finally we add a term to check that **v** started on the correct side of the microsurface (i.e. sidedness agreement) to get the Smith monodirectional shadowing term:

$$G_1(\mathbf{v},\mathbf{m}) = \chi^+\!\left(\frac{\mathbf{v}\cdot\mathbf{m}}{\mathbf{v}\cdot\mathbf{n}}\right) S(\mu) = \chi^+\!\left(\frac{\mathbf{v}\cdot\mathbf{m}}{\mathbf{v}\cdot\mathbf{n}}\right)\frac{1}{1 + \Lambda(\mu)} \qquad (51)$$

Using these equations we can derive G_1 for any microfacet distribution D (though the integral in Equation 48 has no closed form solution for some D) and together with Equation 23 find the corresponding bidirectional shadowing-masking term.

Often another integration over all **m** is performed to get an average shadowing over the whole microsurface, but this is neither needed nor desirable for use with microfacet models.